Journal of International Scientific Publications:
Materials, Methods & Technologies, Volume 7, Part 1
ISSN 1313-2539, Published at: http://www.scientific-publications.net

ELECTRICAL STRESSES OF DC CABLE INSULATION

Cristina Stancu[1], Petru V. Notingher[2]
[1]National Institute for Research&Development in Electrical Engineering INCDIE ICPE CA,
313 Splaiul Unirii Str., Bucharest, Romania
[2]University Politehnica of Bucharest, 313 Splaiul Independentei Str., Bucharest, Romania

Abstract

The DC electric power transmission through power lines represents one of the most important concerns of the electricity producers and users. Unfortunately the polymeric insulated cables have an important disadvantage: the development of a space charge inside the insulation (which modifies the electric field repartition) and especially its long persistence after the voltage switching-off.

In this paper a computation method of the electric field in the homogeneous polymeric insulation of a DC cable is presented. It is assumed that the cable is in operation and some charge layers near the inner and outer semiconducting layers are presented. The computations are done for a medium voltage cable and show that an important local increase of the electric field (near the inner semiconductor layer) is produced. This increase depends on the sign and amount of the charge and on the layer thickness and may lead to the breakdown of the insulation at lower voltages.

Key words: *power cables, lifetime, polyethylene, water trees, failure*

1. INTRODUCTION

High-voltage direct current (HVDC) electric power transmission system uses direct current for the transmission of electrical power (Arrillaga 1998). The most common reason for choosing HVDC over AC transmission is that HVDC is more economic than AC for transmitting large amounts of power over long distances.

Even though HVDC conversion equipment at the terminal stations is costly, overall savings in capital cost may arise because of significantly reduced transmission line costs over long distance routes. HVDC needs fewer conductors than an AC line, as there is no need to support three phases. Also, thinner conductors can be used since HVDC does not suffer from the skin effect. These factors lead to large reductions in power transmission cost for a long distance HVDC system (Hincomni 1996). On the other hand, HVDC transmission losses are quoted as about 3 % per 1,000 km, less than typical losses in an AC transmission system. Generally, DC line losses are 30–40 % less than with AC lines, at the same voltage levels (Wikipedia).

The disadvantages of HVDC are in conversion, switching, control, availability and maintenance. HVDC is less reliable and has lower availability than AC systems, mainly due to the extra conversion equipment (Wikipedia). The required converter stations are expensive and have limited overload capacity. At smaller transmission distances, the losses in the converter stations may be bigger than in an AC transmission line.

An important disadvantage of DC cables represents the existence of the space charge inside the insulation. This charge may appear during the manufacturing processes (breaking of the polymer molecules etc.), thermal and radiative degradation of insulation, charge injection from the electrodes with defects (protuberances etc.) etc. This charge (positive and/or negative) is fixed (on the traps

related with the insulation defects) especially near the semiconducting layers. This may leads to the apparition of some charge layers, whom thickness and densities depend on the content and dimensions of the insulation defects, electric field strength, characteristics of the semiconductor-insulation surfaces, content and dimensions of the water trees etc. (Notingher 2005; Wang et al. 2008; Suh et al. 1994; Li et al. 1997; Li, Fouracre&Crichton 1994; Fouracre, Given&Crichton 1986).

The presence of space charges leads to the modification of the electric field inside the insulation, respectively to its increase near the semi-conductive layer, and to the decrease of the partial discharge and electrical trees inception voltage, making easier the breakdown of the insulation at voltages close to the operating level (Notingher 2005). On the other hand, due to the large relaxation times of the charge in polymers, polymeric insulations are still charged even after the switching-off of the voltage. This leads to the apparition of high electric fields in the cables vicinities, compromising the safety of the operator. For this reason, the computation of the electric field in homogeneous or inhomogeneous (especially that contain water trees) medium or high voltage cable insulation, in the absence or presence of the space charge has been an important research topic (Buller 1967; Stancu et al. 2009; Abou-Dakka, Bulinski&Bamji 2004; Mizutani et al. 2004).

Thus, in (Acedo et al. 2001; Radu et al. 2000; Notingher, Radu&Filippini 2000), the distribution of the electric field has been calculated in the presence of water trees without considering space charges. The electric field computation by the boundary element method in the presence of space charges has been done in (Bamji, Bulinski&Prasad 1993). The calculation of the electric field in electrostatic regime, considering a parabolic variation of the charge density and an exponential variation of the permittivity in water treed areas, is shown in (Stancu et al. 2009; Stancu et al. 2006), where it is considered that water trees are continuous and they have developed either toward the inner semiconductor or the outer semiconductor.

In this paper, the analytical calculation of the electric field in the insulation of a medium voltage cable is presented. If in the previous papers (Stancu, Notingher&Plopeanu 2011; Stancu, Notingher&Plopeanu 2012) it was considered that the insulation contains water trees, in this paper it is assumed that the insulation is homogeneous and contains one or two charge layers (positive or negative) near the inner and outer semi-conductive layers. The values of space charge density used in the calculations have been determined from space charge measurements carried out by the thermal step method (TSM) in flat samples (Notingher jr. et al. 2009).

2. COMPUTATION MODEL

In order to calculate the electric field the cylindrical insulation of a medium voltage cable was considered (Figure 1). The insulation (polyethylene of relative permittivity ε_r) is bounded by the inner semiconductor layer of outer radius r_1 and potential V_1 respectively by the outer semiconductor layer of inner radius r_2 and potential V_2 (Figure 2). It is considered that the insulation contains one or two charge layers (positive or negative) and has a cylindrical shape (of thickness l_c and volume density ρ_v).

As the electrodes but also the charge layers have a cylindrical shape, the electric field is plane parallel (radial). The computation was done in plane domains D having a crown circular shape. The electrostatic regime of the electric field and the cylindrical coordinate system (r, θ, z) with Oz parallel with the axis of the cable were considered. Because the electric field does not depend on the θ and z coordinates, for numerical computation of the potential $V(r)$ and electric field $E(r)$ in a point $P(r)$ from the calculation domain, the following equations were used:

- The Poisson equation:

$$\frac{1}{r}\frac{\partial}{\partial r}\left[r\varepsilon(r)\left(\frac{\partial V(r)}{\partial r}\right)\right]=-\rho_v(r) \quad (1)$$

- The theorem of electrostatic potential:

$$E(r)=-\frac{\partial V(r)}{\partial r}, \quad (2)$$

where the permittivity $\varepsilon(r)$ and the volume space charge density $\rho_v(r)$ are known in each point $P(r)$ inside the insulation (Stancu 2008).

Boundary (at the interfaces between the semi-conductive layers and insulation) and the source conditions (volume charge density values near the semi-conductive layers) are added to the equations (1) and (2).



Fig. 1. Medium voltage cable: 1 – Conductor, 2 – Inner semiconductor layer, 3 – Insulation, 4 – Outer semiconductor layer, 5 – Sheath, 6 – Jacket.

3. COMPUTATION OF THE ELECTRIC FIELD

The numerical computation of the electric field was done for three computation domains D, with the charge layers: a) near the inner semiconductor layer, b) near the outer semiconductor layer and c) near both the semi-conductive layers.

3.1. *Charge layer near the inner semi-conductive layer*

3.1.1. *Computation domain*

The computation domain D is presented in the Figure 2. It consists of two sub-domains: D_1 where a charge layer has developed (of known average density ρ_{vmed}), bounded by the cylindrical surfaces S_1 (of radius r_1) and S_2 (of radius $r_1 + l_c$, l_c representing the charge layer thickness) and sub-domain D_2 without charge, bounded by the surfaces S_2 and S_3 (of radius r_2). The numerical computations were done for $l_c \in [0.1...1]$ mm, $\varepsilon_1(r) = \varepsilon_2(r) = 2.2\ \varepsilon_0$, $\varepsilon_0 = 8.85\text{x}10^{-12}$ F/m, $\rho_{vmed} \in [-0.1...+0.2]$ C/m^3 and $V_1 = 20$ kV.

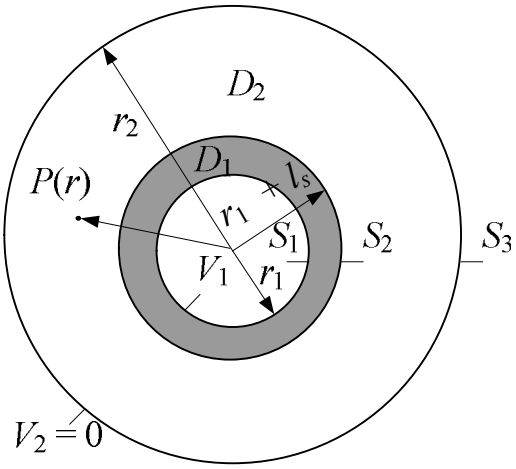


Fig. 2. Computation domain of the electric field in the presence of a charge layer near the inner semiconductor layer.

The charge density in the sub-domain D_1 – $\rho_v(r)$ – was considered either constant ($\rho_v = \rho_v(r) = -0.1...+0.2$ C/m^3), or parabolic variable with r-coordinate, respectively:

$$\rho_v(r) = \rho_{v0}\left(ar^2 + br + e\right),$$

where ρ_{v0} represents the charge density value near the inner semiconductor layer and a, b and e are calculated.

Using the condition that the total charge Q_1 contained in a region with the length and section identical to the one of the sub-domain D_1, in the case of a constant charge ρ_{vmed} (Figure 3):

$$Q_1 = \rho_{vmed}\pi\left[(r_1 + l_c)^2 - r_1^2\right]$$

to be equal to the one of a variable charge density ρ_v, respectively Q_1':

$$Q_1' = \int_{r_1}^{r_1+l_c} \rho_{v0}\left(ar^2 + br + e\right)\pi r^2 \mathrm{d}r\,.$$

the values of ρ_{v0} were calculated.

It results:

ISSN 1313-2539, Published at: http://www.scientific-publications.net

$$\rho_{v0} = \rho_{vmed} \frac{(r_1 + l_c) - r_1^2}{\int_{r_1}^{r_1+l_c} (ar^4 + br^3 + er^2)} dr \quad (3)$$

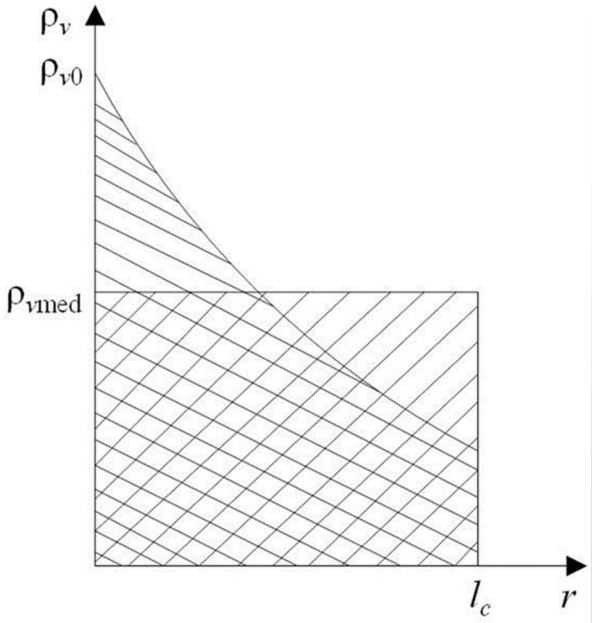


Fig. 3. Variation of the charge density ρ_v with the r – coordinate in the sub-domain D_1.

3.1.2. *Equations*

Boundary and the crossing conditions are added to the equations (1) and (2) as follows:

- Boundary conditions

$$V(P) = V_1,\ P \in S_1$$
$$V(P) = V_2 = 0,\ P \in S_2 \quad (4)$$

- Crossing conditions on the surface S_2:

$$V_1(P) = V_2(P),\ P \in S_2$$
$$\frac{dV_1(P)}{dr} = \frac{dV_2(P)}{dr},\ P \in S_2, \quad (5)$$

where V_1 (P) and V_2 (P) represents the values of the potential in the point $P \in S_2$, computed with the expressions corresponding to the sub-domains D_1 and D_2.

3.1.3. *Equations of the potential and electric field*

Using the equations (1), (2), (4) and (5) the equations of the potential and electric field were obtained:

$$V_1(r) = -\frac{\rho_{v0}}{\varepsilon_1}\left(a_1\frac{r^4}{16} + b_1\frac{r^3}{9} + e_1\frac{r^2}{4}\right) + C_1 \ln r + C_2$$
$$E_1(r) = \frac{\rho_{v0}}{\varepsilon_1}\left(a_1\frac{r^3}{4} + b_1\frac{r^2}{3} + e_1\frac{r}{2}\right) - \frac{C_1}{r} \quad (6)$$
$$V_2(r) = C_3 \ln r + C_4$$
$$E_2(r) = -\frac{C_3}{r}$$

the values of the constants a_1, b_1, e_1, $C_1 \ldots C_4$ being presented in the Annex 1 (Stancu 2008).

3.1.4. *Results*

3.1.4.1. *Positive charge case* ($\rho_{vmed} > 0$)

Figure 4 is concerned with the variation of the electric field E with respect to the coordinate r in the absence and in the presence of a positive charge layer. It comes out that the presence of the charge near the inner semi-conductive layer leads to the decrease of the electric field in this area and to its increase in the outer area. The maximum electric field value is obtained at the tip of the charge layer. For l_c = 1 mm, $E_{max} = E$ (9 mm) = 5.064 MV/m with 10.64 % higher than its value in the absence of the charge layer.

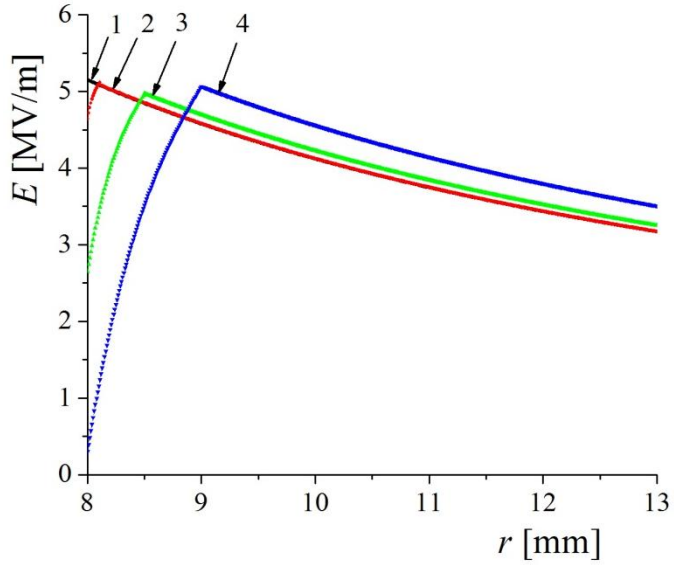


Fig. 4. Variation of the electric field E with the r – coordinate in the absence (1) and presence of a positive charge layer with l_c = 0.1 mm (2), l_c = 0.5 mm (3) and l_c = 1 mm (4) (ρ_{vmed} = + 0.106 C/m^3, V_1 = 20 kV).

Increasing the charge layer thickness, the electric field E decreases near the inner semi-conductive layer (from 4.638 MV/m for l_c = 0.1 mm to 0.304 MV/m for l_c =1 mm) but also at the tip of the charge layer (from 5.064 MV/m for l_c =0.1 mm to 5 MV/m for l_c = 1 mm). Near the outer semi-conductive layer the electric field E increases (from 3.172 MV/m for l_c =0.1 mm to 3.506 MV/m for l_c =1 mm) (Figure 5).

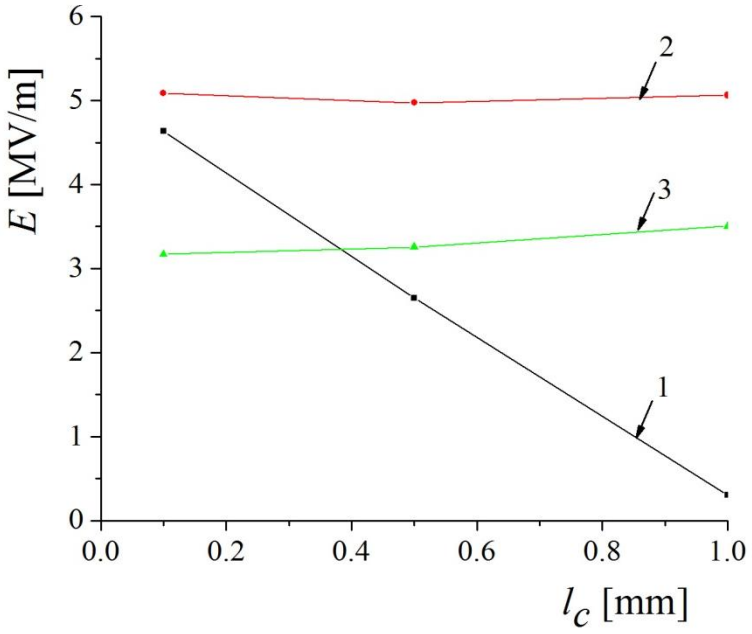


Fig. 5. Variation of the electric field E with the charge layer thickness l_c: near the inner semi-conductive layer (1), at the tip of the charge layer (2) and near the outer semi-conductive layer (3) (ρ_{vmed} = + 0.106 C/m^3, V_1 = 20 kV).

Increasing the ρ_{vmed} values (from 0.106 C/m^3 to 0.2 C/m^3) the electric field E decreases near the inner semi-conductive layer (from 3.638 MV/m to – 15.5 MV/m) and increases at the tip of the charge layer (from 4.923 MV/m to 5,952 MV/m) and near the outer semi-conductive layer (from 3.218 MV/m to 3.891 MV/m) (Figure 6).

3.1.4.2. *Negative charge case* ($\rho_{vmed} < 0$)

Figure 7 is concerned with the variation of the electric field E with respect to the coordinate r in the case of a negative charge existence. It comes out that the charge presence near the inner semi-conductive layer leads to the increase of E in this area and to its decrease in the outer area. Therefore, for l_c = 1 mm and ρ_{vmed} = - 0.106 C/m^3, the electric field value E is 94.5 % higher than in the charge absence.

The values of E increase with l_c near the inner semi-conductive layer (from 5.66 MV/m for l_c = 0.1 mm to 9.993 MV/m for l_c =1 mm) and to its decrease at the tip of the charge layer (from 5.08 MV/m for l_c = 0.1 mm to 4.089 MV/m for l_c = 1 mm) and near to the outer semi-conductive layer (from 3.165 MV/m for l_c = 0.1 mm to 2.831 MV/m for l_c = 1 mm) (Figure 8).

ISSN 1313-2539, Published at: http://www.scientific-publications.net

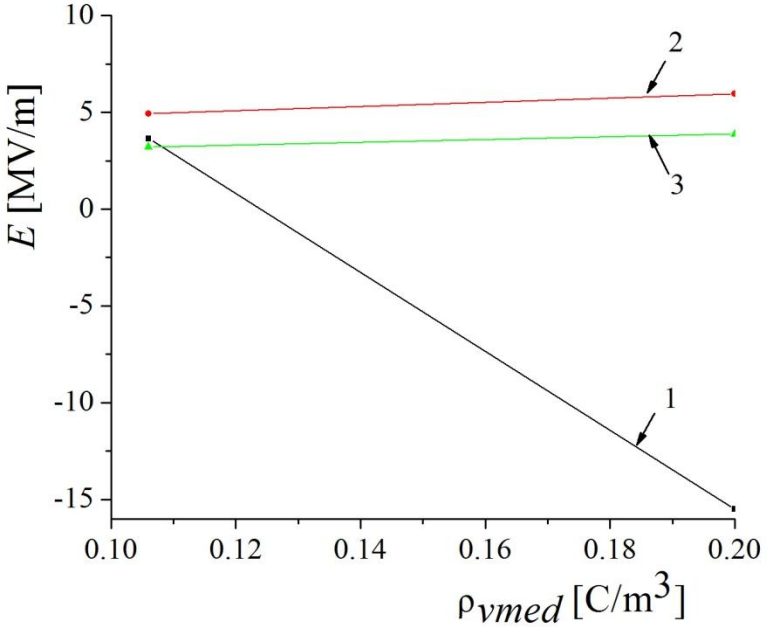


Fig. 6. Variation of the electric field E with the average charge density ρ_{vmed}: near the inner semi-conductive layer (1), at the tip of the charge layer (2) and near the outer semi-conductive layer (3) (l_c = 0.5 mm, V_1 = 20 kV).

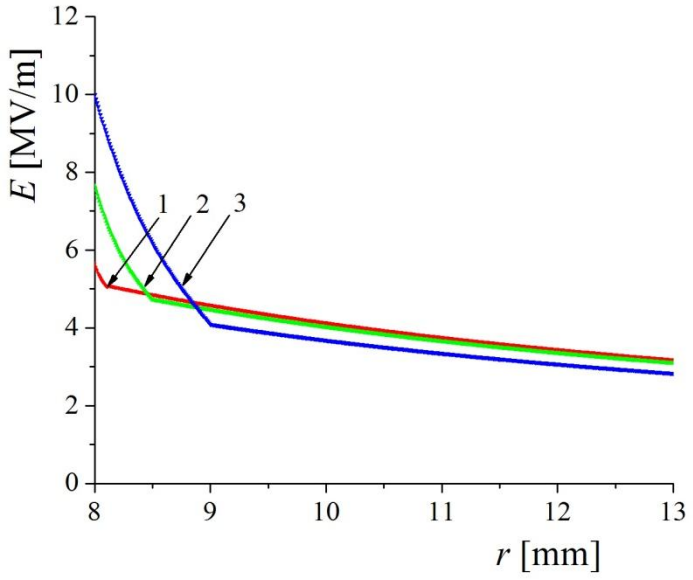


Fig. 7. Variation of the electric field E with the r – coordinate in the presence of a negative charge layer with l_c = 0.1 mm (1), l_c = 0.5 mm (2) and l_c = 1 mm (3) (ρ_{vmed} = - 0.106 C/m^3, V_1 = 20 kV).

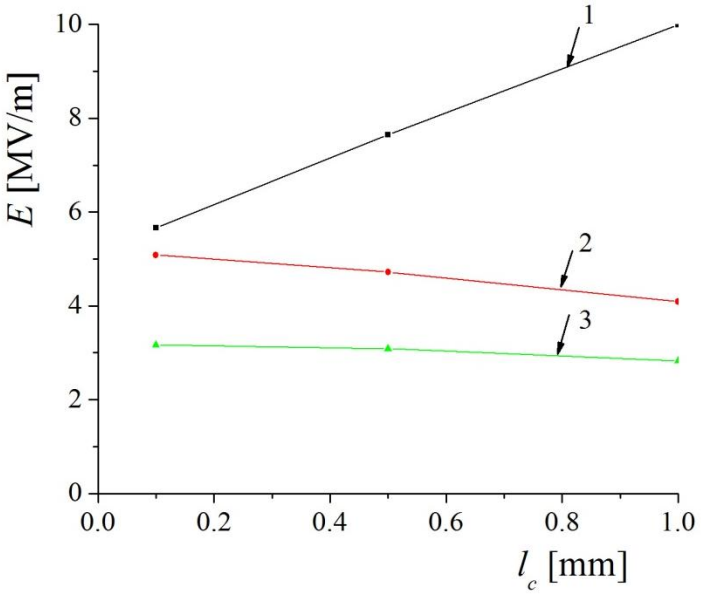


Fig. 8. Variation of the electric field E with the charge layer thickness l_c: near the inner semi-conductive layer (1), at the tip of the charge layer (2) and near the outer semi-conductive layer (3) (ρ_{vmed} = - 0.106 C/m^3, V_1 = 20 kV).

3.2. *Charge layer near the outer semi-conductive layer*

3.2.1. *Computation domain*

Figure 9 is concerned with the computation domain D which contains the charge layer near the outer semi-conductor. It consists of two sub-domains: D_1 (without charge), bounded by the cylindrical surfaces S_1 (of radius r_1) and S_2 (of radius r_2 - l_c, l_c representing the charge layer thickness) and D_2 (with charge), bounded by the surfaces S_2 and S_3 (of radius r_2). The numerical computations were done for $l_c \in [0.1...1]$ mm, $\rho_{vmed} \in [- 0.1...+ 0.2]$ C/m^3 and V_1 = 20 kV.

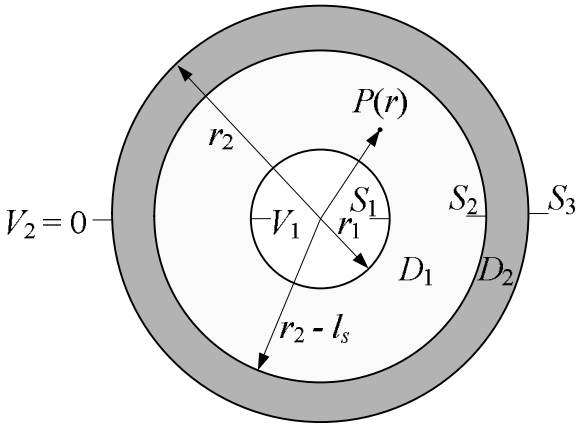


Fig. 9. Computation domain of the electric field in the presence of a charge layer near the outer semiconductor.

3.2.2. *Equations*

The crossing conditions on the surface S_2 are added to the equations (1), (2) and (4):

$$V_1(P) = V_2(P),\ P \in S_2$$
$$\frac{dV_1(P)}{dr} = \frac{dV_2(P)}{dr},\ P \in S_2, \quad (7)$$

where V_1 (P) and V_2 (P) are the values of the potential in the point $P \in S_2$ computed with the corresponding equations of the sub-domains D_1 and D_2.

3.2.3. *Equations of the potential and electric field*

From (1), (2), (4) and (7) the equations of the potential and electric field in the sub-domains D_1 and D_2 were obtained:

$$V_1(r) = C_1 \ln r + C_2$$
$$E_1(r) = -\frac{C_1}{r} \quad (8)$$
$$V_2(r) = -\frac{\rho_{v0}}{\varepsilon_2}\left(a_2\frac{r^4}{16} + b_2\frac{r^3}{9} + e_2\frac{r^2}{4}\right) + C_3 \ln r + C_4$$
$$E_2(r) = \frac{\rho_{v0}}{\varepsilon_2}\left(a_2\frac{r^3}{4} + b_2\frac{r^2}{3} + e_2\frac{r}{2}\right) - \frac{C_3}{r},$$

values of the constants a_2, b_2, e_2, $C_1 ... C_4$ being presented in the Annex 2 (Stancu 2008).

3.2.4. *Results*

3.2.4.1. *Positive charge case* ($\rho_{vmed} > 0$)

Figure 10 is concerned with the variation of the electric field E with respect to the coordinate the r for positive charge layers of different thicknesses. It comes out that the presence of a charge layer near the outer semiconductor leads to the increase of the electric field in this area ant to its decrease in the outer area. Therefore, for ρ_{vmed} = 0.106 C/m^3, the electric field value in the coordinate point r = 13 mm is 115.8 % higher than its value in the absence of the charge layer

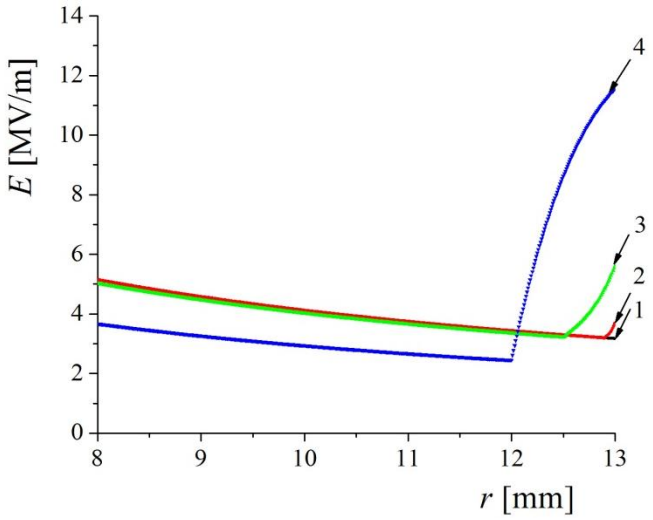


Fig. 10. Variation of the electric field E with the r-coordinate in the absence (1) and presence of a positive charge layer with l_c = 0.1 mm (2), l_c = 0.5 mm (3) and l_c = 1 mm (4) (ρ_{vmed} = + 0.106 C/m^3, V_1 = 20 kV).

Figure 11 is concerned with the variation of E with respect to the charge layer thickness l_c – for ρ_{vmed} = 0.106 C/m^3. It comes out that increasing the charge layer thickness, the electric field decrease near the inner semi-conductive layer (from 5.143 MV/m for l_c = 0.1 mm to 3.672 MV/m for l_c = 1 mm) and at the tip of the charge layer (from 3.19 MV/m for l_c = 0.1 mm to 2.44 MV/m for l_c = 1 mm) and to its increase near the outer semi-conductive layer (from 3.67 MV/m for l_c = 0.1 mm to 11.564 MV/m for l_c = 1 mm).

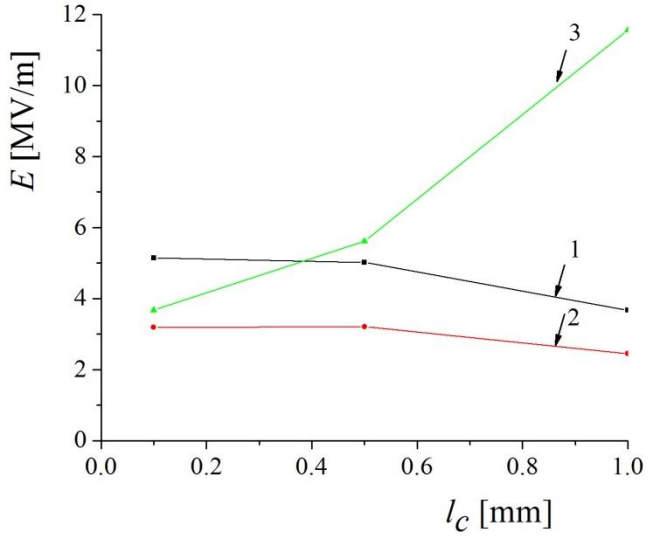


Fig. 11. Variation of the electric field E with the charge layer thickness l_c: near the inner semi-conductive layer (1), at the tip of the charge layer (2) and near the outer semi-conductive layer (3) (ρ_{vmed} = + 0.106 C/m^3, V_1 = 20 kV).

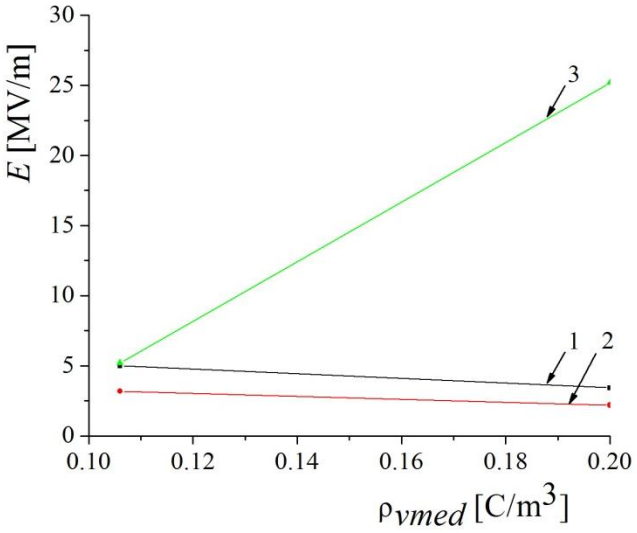


Fig. 12. Variation of the electric field E with average charge density ρ_{vmed}: near the inner semi-conductive layer (1), at the tip of the charge layer (2) and near the outer semi-conductive layer (3) (l_c = 0.5 mm, V_1 = 20 kV).

Increasing the values of ρ_{vmed}, the electric field E decreases near the inner semi-conductive layer (from 4.992 MV/m to 3.42 MV/m) and at the tip of the charge layer (from 3.195 MV/m to 2.2 MV/m) and at its increase near the outer semi-conductive layer (from 5.199 MV/m to 25.2 MV/m) (Figure 12).

3.2.4.2. *Negative charge case* ($\rho_{vmed} < 0$)

In the presence of a charge layer near the outer semi-conductive layer, the electric field E increases significantly near the inner semi-conductive layer and decreases near the outer one reversing even its sign (Figure 13). This phenomenon, appropriate to DC cables, was also obtained by Bodega (Bodega 2006) which explain it by the increase, about 12 %, of the homo-charges (+ 22.5 kV), when the difference between the conductor and sheath temperature is 20 ºC.

Increasing the negative charge layer thickness values, the electric field increases near the inner semi-conductive layer (Figure 14, curve 1) and at the tip of the charge layer (Figure 14, curve 2) and to its decrease near the outer semi-conductive layer (Figure 14, curve 3).

3.3. *Charge near both semi-conductive layers*

3.3.1. *Computation domain*

Figure 15 is concerned with the computation domain D which contains two charge layers. It contains three sub-domains: D_1 (with $\rho_{vmed1} \neq 0$ and $\varepsilon_1 = 2.2\ \varepsilon_0$), bounded by the cylindrical surfaces S_1 (of radius r_1) and S_2 (of radius $r_1 + l_{c1}$), sub-domain D_2 (with $\rho_{vmed} = 0$ and $\varepsilon_2 = 2.2\ \varepsilon_0$), bounded by the surfaces S_2 and S_3 (of radius $r_2 - l_{c2}$) and D_3 (with $\rho_{vmed} \neq 0$ and $\varepsilon_3 = 2.2\ \varepsilon_0$), bounded by the cylindrical surfaces S_3 and S_4 (of rayon r_2). For space charge density ρ_v (r) the following variation laws were considered:

$$\rho_v(r) = \rho_{v0}\left(a_1 r^2 + b_1 r + e_1\right)$$

in D_1 and

ISSN 1313-2539, Published at: http://www.scientific-publications.net

$$\rho_v(r) = \rho_{v0}\left(a_2 r^2 + b_2 r + e_2\right)$$

in D_2.

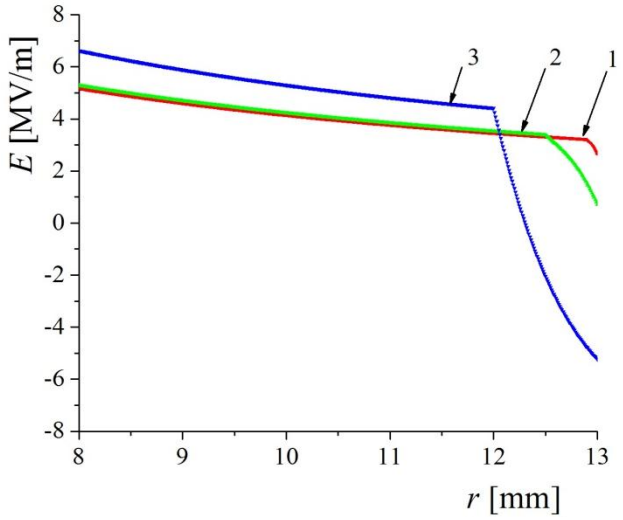


Fig. 13. Variation of the electric field E with the r – coordinate in the presence of a negative charge layer with l_c = 0.1 mm (1), l_c = 0.5 mm (2) and l_c = 1 mm (3) (ρ_{vmed} = - 0.106 C/m^3, V_1 = 20 kV).

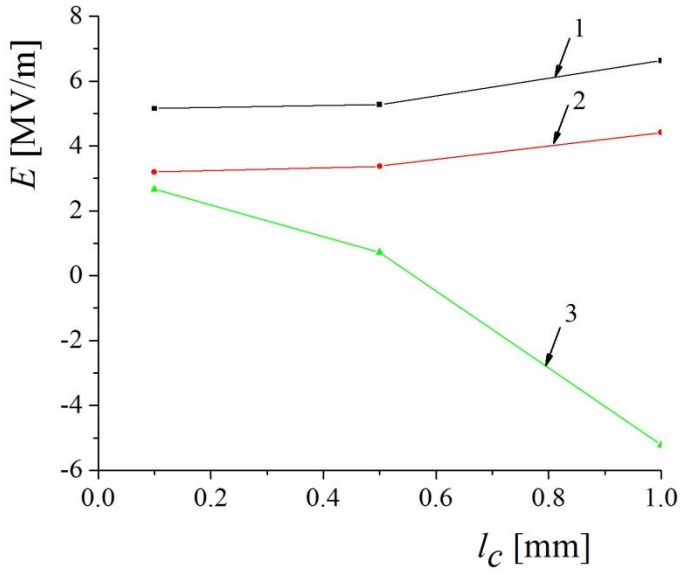


Fig. 14. Variation of the electric field E with the charge layer thickness l_s: near the inner semi-conductive layer (1), at the tip of the charge layer (2) and near the outer semi-conductive layer (3) (ρ_{vmed} = - 0.106 C/m^3, V_1 = 20 kV).

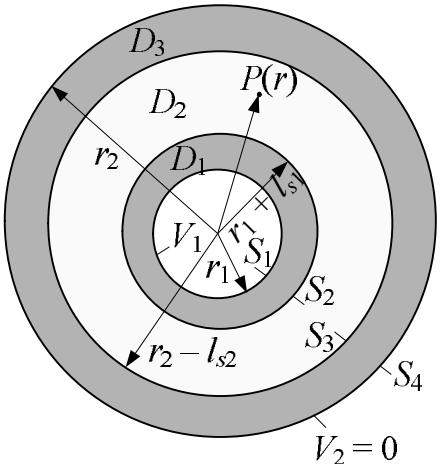


Fig. 15. Computation domain of the electric field in the presence of two charge layers near the inner and outer semiconductor.

3.3.2. *Equations*

Crossing conditions on the surfaces S_2 and S_3 are added to the equations (1), (2) and (4):

$$\begin{aligned} &V_1(P) = V_2(P),\ P \in S_2 \\ &\frac{\mathrm{d}V_1(P)}{\mathrm{d}r} = \frac{\mathrm{d}V_2(P)}{\mathrm{d}r},\ P \in S_2 \\ &V_2(P) = V_3(P),\ P \in S_3 \\ &\frac{\mathrm{d}V_2(P)}{\mathrm{d}r} = \frac{\mathrm{d}V_3(P)}{\mathrm{d}r},\ P \in S_3 \end{aligned} \tag{9}$$

where $V_1(P)$, $V_2(P)$ and $V_3(P)$ are the values of the potential in the points $P \in S_{2,3}$ computed with the corresponding equations of the sub-domains D_1, D_2 and D_3.

3.3.3. *Equations of the potential and electric field*

From (1), (2), (4) and (9) the following equations were obtained:

$$V_1(r) = -\frac{\rho_{v0}}{\varepsilon_1}\left(a_1\frac{r^4}{16} + b_1\frac{r^3}{9} + e_1\frac{r^2}{4}\right) + C_1 \ln r + C_2$$

$$E_1(r) = \frac{\rho_{v0}}{\varepsilon_1}\left(a_1\frac{r^3}{4} + b_1\frac{r^2}{3} + e_1\frac{r}{2}\right) - \frac{C_1}{r}$$

ISSN 1313-2539, Published at: http://www.scientific-publications.net

$$V_2(r) = C_3 \ln r + C_4$$
$$E_2(r) = -\frac{C_3}{r} \qquad (10)$$
$$V_3(r) = -\frac{\rho_{v0}}{\varepsilon_3}\left(a_2\frac{r^4}{16} + b_2\frac{r^3}{9} + e_2\frac{r^2}{4}\right) + C_5 \ln r + C_6$$
$$E_3(r) = \frac{\rho_{v0}}{\varepsilon_3}\left(a_2\frac{r^3}{4} + b_2\frac{r^2}{3} + e_2\frac{r}{2}\right) - \frac{C_5}{r},$$

values of the constants a_1, b_1, a_2, b_2, e_1, e_2, $C_1 ... C_6$ being presented in the Annex 3 (Stancu 2008).

3.3.4. *Results. Discussion*

Figure 16 is concerned with the variation of the electric field E with respect to the coordinate r for two positive charge layers of thicknesses $l_{c1} = l_{c2} = l_c \in [0.1...1]$ mm and $\rho_{vmed} = 0.106$ C/m^3. It comes out that the electric field E decreases near the inner semi-conductive layer and increases the outer semi-conductive layer (Figure 16, curves 3 and 4). These variations are more important with the increase of l_c (Figure 17, curves 1 and 4). Therefore, for $l_{c1} = l_{c2} = l_c = 1$ mm, E values increases with 158.4 % to those in the absence of the charge reaching to 8.166 MV/m.

As a consequence, the probability of partial discharge and electrical trees inception increases leading to a breakdown of the insulation.

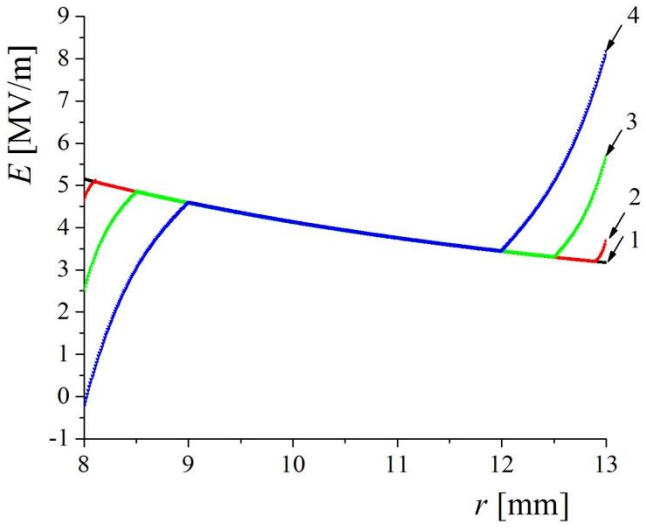


Fig. 16. Variation of the electric field E with the r – coordinate in the absence (1) and presence of charge layers with $l_c = 0.1$ mm (2), $l_c = 0.5$ mm (3) and $l_c = 1$ mm (4) ($\rho_{vmed} = +0.106$ C/m^3, $V_1 = 20$ kV).

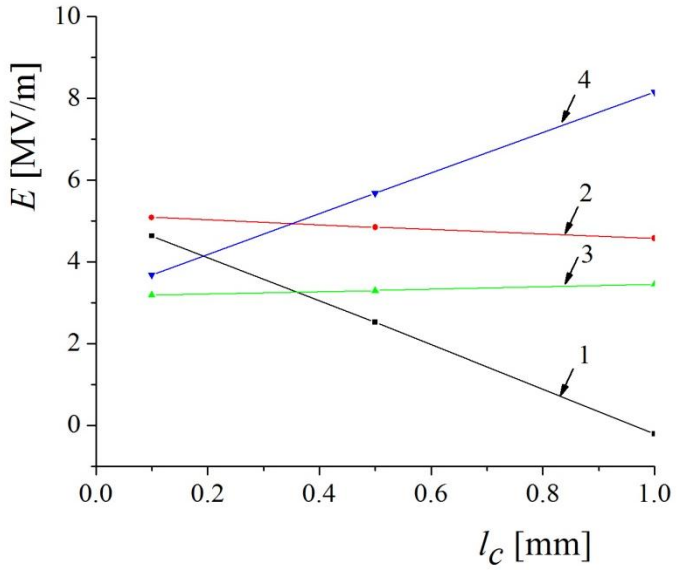


Fig. 17. Variation of the electric field E with the charge layer thickness l_c: near the inner semi-conductive layer (1), at the tip of the charge layer with the thickness $l_{c1} = l_c$ (2), at the tip of the charge layer with the thickness $l_{c2} = l_c$ (3) and near the outer semi-conductive layer (4) (ρ_{vmed} = + 0.106 C/m^3, V_1 = 20 kV).

4. CONCLUSIONS

Considering charge layers near the semi-conductive layers and having a constant or parabolic variable charge density with respect to the axis of the cable, relatively simple expressions of the electric field were obtained.

The electric field modify in the presence of space charge, depending on the position and layer thickness, but also on their sign and of the applied potentials to semi-conductive layers.

The maximum values of the electric field increases considerably with the charge density and layer thickness, two times higher than in the absence of the charge. Therefore, the probability of partial discharges and electrical trees inception at lower voltages increases. As a consequence, the probability of the insulation breakdown at nominal voltage increases.

The electric field computation in DC cable insulation in the presence of the space charge, considering the electro-kinetic quasi-stationary regime will be presented in a future paper.

REFERENCES

1. Arrillaga, J 1998, *High Voltage Direct Current Transmission*, Second Edition, Institution of Electrical Engineers, London.
2. Hincomni, N 1996, 'High-Voltage DC Transmission', *IEEE SPECTRUM*, pp. 63-72.
3. http://en.wikipedia.org/wiki/High-voltage_direct_current.
4. Notingher, P V 2005, *Materials for Electrotechnics*, Politehnica Press, Bucharest.

5. Wang, X, Yoshimura, N, Tu, D, Tanaka, Y, Takada, T 1998, 'Distribution Characteristics and Formation Mechanism of Space Charge in PE Materials', *Proceedings of IEEE International Symposium of Electrical Insulation*, pp. 119-112.
6. Suh, K S, Hwang, S J, Noh, J S, Tanaka, T 1994, 'Effects of constituents of XLPE on the formation of space charge', *IEEE Transactions on Dielectrics and Electrical Insulation*, vol. 1, no. 6, pp. 1077–1083.
7. Li, Y, Kawai, J, Ebinuma, Y, Fujiwara, Y, Tanaka, Y, Takada, T 1997, 'Space charge behavior under ac voltage in water-treed PE observed by the PEA method', *IEEE Transactions on Dielectrics and Electrical Insulation*, vol. 4, no. 1, pp. 52–57.
8. Li, H M, Fouracre, R A, Crichton, B H 1994, 'The influence of ions on thermally stimulated discharge current spectra of water-treed additive free low-density polyethylene', *IEEE Transactions on Dielectrics and Electrical Insulation*, vol. 1, no. 6, pp. 1084–1093.
9. Fouracre, R A, Given, M J, Crichton, B H 1986, 'The effect of alternating electric fields on ion migration in solid dielectrics', *Journal of Physical Chemistry: Solid State Physics.*, vol. 19, no. 12, pp. 1949–1958.
10. Buller, F H 1967, 'Calculation of Electrical Stresses in DC Cable Insulation', *IEEE Power Applied Systems*, vol. 86, pp. 1169-1178.
11. Stancu, C, Notingher, P V, Ciuprina, F, Notingher, P jr, Agnel, S, Castellon, J, Toureille, A 2009, 'Computation of the Electric Field in Cable Insulation in the Presence of Water Trees and Space Charge', *IEEE Transactions on Industry Applications*, vol. 45, no. 1, pp. 30-49.
12. Abou-Dakka, M, Bulinski, A, Bamji, S 2004, 'Space charge development and breakdown in XLPE under DC field', *IEEE Transactions on Dielectrics and Electrical Insulation*, vol. 11, no. 1, pp. 41–49.
13. Mizutani, T, Semi, H, Kaneko, K., Mori, T, Ishioka, M 2000, 'Space charge and field distributions in low-density polyethylene', *Proceedings of IEEE International Symposium on Electrical Insulation*, pp. 493–496.
14. Acedo, M, Radu, I, Frutos, F, Filippini, J C, Notingher, P V 2001, 'Water treeing in underground power cables: Modelling of the trees and calculation of the electric field perturbation', *Journal of Electrostatics*, vol. 53, no. 4, pp. 267– 294.
15. Radu, I, Acedo, M, Filippini, J C, Notingher, P V, Frutos, F 2000, 'The effect of water treeing on the electric field distribution of XLPE: Consequences on the dielectric strength', *IEEE Transactions on Dielectrics and Electrical Insulation*, vol. 17, no. 6, pp. 860–868.
16. Notingher, P V, Radu, I, Filippini, J C 2000, 'Numerical method of computation of the electric field in insulation with water-trees', *Revue Roumaine des Sciences Technique—Electrotechnique et Energetique*, vol. 45, no. 2, pp. 221–236.
17. Bamji, S S, Bulinski, A T, Prasad, K M 1993, 'Electric field calculations with the boundary element method', *IEEE Transactions on Dielectrics and Electrical Insulation*, vol. 28, no. 3, pp. 420–424.
18. Stancu, C, Notingher, P V, Ciuprina, F, Notingher, P Jr., Agnel, S, Castellon, J, Toureille, A 2006, 'Electric field computation in water treed polyethylene with space charge accumulation', *Proceedings of IEEE International Symposium on Electrical Insulation*, pp. 186–189.

19. Stancu, C, Notingher, PV, Plopeanu, MG 2011, 'Influence of Water Trees on Breakdown Voltage of Polymeric Cables Insulations', *Journal of International Scientific Publications: Materials, Methods & Technologies,* vol. 5, part 2, pp. 101-116.
20. Stancu, C, Notingher, P V, Plopeanu, MG 2012, 'Electrical Lifetime Estimation of Underground Power Cables', *Journal of International Scientific Publications: Materials, Methods & Technologies*, vol. 6, part 1, pp. 165 – 178.
21. Notingher, P jr., Toureille, A, Agnel, S, Castellon, J 2009, 'Determination of Electric Field and Space Charge in the Insulation of Power Cables With the Thermal Step Method and a New Mathematical Processing', *IEEE Transactions on Industry Applications*, vol. 45, no. 1, pp. 67 - 74.
22. Stancu, C 2008, 'Caractérisation de l'état de vieillissement des isolations polymères par la mesure d'arborescences et des charge d'espace', PhD Thesis, University Politehnica of Bucharest – Université Montpellier 2.
23. Bodega, R 2006, 'Space Charge Accumulation in Polymeric High Voltage DC Cable Systems', PhD Thesis, Delft University of Technology.